



UNIVERSITY OF LEEDS

This is a repository copy of *Quantum Transmission Line Modelling and Experimental Investigation of the Output Characteristics of a Terahertz Quantum Cascade Laser*.

White Rose Research Online URL for this paper:  
<http://eprints.whiterose.ac.uk/155828/>

Version: Accepted Version

---

**Article:**

Xia, M, Rubino, P [orcid.org/0000-0001-8669-6747](https://orcid.org/0000-0001-8669-6747), Li, LH [orcid.org/0000-0003-4998-7259](https://orcid.org/0000-0003-4998-7259) et al. (5 more authors) (2020) Quantum Transmission Line Modelling and Experimental Investigation of the Output Characteristics of a Terahertz Quantum Cascade Laser. IEEE Transactions on Terahertz Science and Technology, 10 (4). pp. 333-342. ISSN 2156-342X

<https://doi.org/10.1109/TTHZ.2020.2970341>

---

(c) 2019 IEEE. Personal use of this material is permitted. Permission from IEEE must be obtained for all other uses, in any current or future media, including reprinting/republishing this material for advertising or promotional purposes, creating new collective works, for resale or redistribution to servers or lists, or reuse of any copyrighted component of this work in other works.

**Reuse**

Items deposited in White Rose Research Online are protected by copyright, with all rights reserved unless indicated otherwise. They may be downloaded and/or printed for private study, or other acts as permitted by national copyright laws. The publisher or other rights holders may allow further reproduction and re-use of the full text version. This is indicated by the licence information on the White Rose Research Online record for the item.

**Takedown**

If you consider content in White Rose Research Online to be in breach of UK law, please notify us by emailing [eprints@whiterose.ac.uk](mailto:eprints@whiterose.ac.uk) including the URL of the record and the reason for the withdrawal request.



[eprints@whiterose.ac.uk](mailto:eprints@whiterose.ac.uk)  
<https://eprints.whiterose.ac.uk/>

# Quantum Transmission Line Modelling and Experimental Investigation of the Output Characteristics of a Terahertz Quantum Cascade Laser

Mingjun Xia, Pierluigi Rubino, Lianhe Li, Iman Kundu, Alexander Valavanis, Alexander Giles Davies, Edmund H. Linfield, and Paul Dean

**Abstract**—We describe a new approach to modelling the optoelectronic properties of a terahertz-frequency quantum cascade laser (THz QCL) based on a quantum transmission line modelling (Q-TLM) method. Parallel quantum cascade transmission line modelling units are employed to describe the dynamic optical processes in a nine-well THz QCL in both the time and frequency domains. The model is used to simulate the current–power characteristics of a QCL device and good agreement is found with experimental measurements, including an accurate prediction of the threshold current and emitted power. It is also confirmed that the Q-TLM model can accurately predict the Stark-induced blue shift of the emission spectrum of the THz QCL with increasing injection current. Furthermore, we establish the new Q-TLM model to describe the properties of a THz QCL device incorporating a photonic lattice patterned on the laser ridge, by linking the transmission line structure to each scattering module. The predicted effects of the lattice structure on the steady-state emission spectra of the THz QCL, including the side-mode suppression, are found to be in good agreement with experimental results. Our Q-TLM modelling approach is a promising tool for the future design of THz QCLs and analysis of their temporal and spectral behaviors.

**Index Terms**—Terahertz quantum cascade laser, Transmission line modelling, temporal and spectral analysis, photonic lattice

## I. INTRODUCTION

Manuscript received May. 2019; revised Nov. 2019; accepted Jan. 2020.

This work was supported by the National Natural Science Foundation of China(61905217), Natural Science Foundation of Zhejiang Province (LQ19F040010), Fundamental Research Funds for Central Universities of China (ZJU: 2018QNA5008), the Engineering and Physical Sciences Research Council (EPSRC),UK (HyperTerahertz programme EP/P021859/1) and the European Union FET-Open grant ULTRAQCL 665158. (Corresponding author: Mingjun Xia)

M. Xia is with the College of Information Science and Electronic Engineering, Zhejiang University, Hangzhou 310027, China (e-mail: xiamingjun@zju.edu.cn).

P. Rubino, L. Li, I. Kundu, A. Valavanis, A.G. Davis, E.H. Linfield and P. Dean are with the School of Electronic and Electrical Engineering, University of Leeds, Leeds, LS2 9JT, U.K. (email:elpr@leeds.ac.uk, L.H.Li@leeds.ac.uk; i.kundu@leeds.ac.uk; a.valavanis@leeds.ac.uk; e.h.linfield@leeds.ac.uk; G.Davies@leeds.ac.uk; P.Dean@leeds.ac.uk)

Terahertz-frequency quantum cascade lasers (THz-QCLs) have established themselves as the one of the most promising compact sources of high power THz radiation suited to a range of applications [1-4]. The ability to control the electronic wavefunctions in these devices via engineering of the quantum heterostructure offers a high degree of design freedom for achieving lasing in the frequency range ~1-5 THz[4-7]. Knowing the temporal and spectral dynamics of THz QCL enables us to understand the complex behavior of THz QCL and optimize the structure design. Furthermore, analysis of the temporal and spectral output of THz QCL is significantly important for promoting its applications in spectroscopy [8], security detection [9]and THz communication [10].

However, there is a lack of a suitable apparatus for second-order autocorrelation measurements to provide this information in the THz range. THz time-domain spectroscopy (TDS) and Fourier transform infrared spectrometry (FTIR) have been employed to measure the output of THz QCLs in the time and frequency domains, respectively. However, the frequency-resolution of most FTIR systems is insufficient to measure small wavelength shifts and analyze the precise multimode behavior of THz QCL. High-resolution spectroscopy in the THz range is also poorly developed, owing to the lack of integrated, high-power THz sources [11]. Therefore, an effective THz-QCL model is highly desirable for analyzing the output properties of THz-QCLs in the time and frequency domains.

Various approaches have been adopted to model the optoelectronic properties of quantum cascade lasers including rate-equation approaches [12], Monte-Carlo simulations [13], density matrix models [14-15], Green's function calculations [16] and pure quantum-mechanical models [17]. Simple models based on reduced rate equations are able to qualitatively predict the output power of THz-QCLs varying with the injection current but they cannot simulate the dynamic output waveforms of THz-QCL in the time and frequency domains [18-19]. Some physical mechanisms or waveguide structure design, such as gain modulation or coupled cavity structure, can lead to spectral tuning and the variation of electric field modes [20]. While the spectral variation and multi-mode behavior cannot be explained

by conventional rate-equations approaches. other sophisticated quantum mechanical models are computationally intensive. Progress has been achieved with respect to modelling THz QCL. In Ref [21], S. Kohen et al. employed the two- and three-dimensional electromagnetic finite-element method to model and analyze the waveguide and resonators in THz QCL; E. Dupont et al. developed a simplified density-matrix model for THz QCL by describing the populations of different subbands and the coherence terms, which gives the correct order of magnitude of current density [22]; R. Terazz and J. Faist presented a transport model for quantum cascade laser based on density matrix formalism by incorporating the optical field so that the model can be used to find the current–voltage and current–optical power characteristics of quantum cascade laser [23]; P. Tzenov et al. present a theoretical model for THz QCL by employing a full numerical solution of Maxwell-Bloch equations, which is effectively used to investigate the frequency comb generation[24]; X. Qi et al. analysed the mode selection and frequency tuning capability of coupled-cavity THz QCLs by using a scattering matrix method and multimode reduced rate equations[25]; In Ref. [26], C. Jirauschek and T. Kubis gave a systematic review of the modeling techniques used for the simulation of quantum cascade lasers.

Recently, we proposed a new theoretical modelling technique-quantum transmission line modelling (Q-TLM) method applicable to semiconductor optical devices [27]. Q-TLM is a general modelling method that establishes models from describing the basic photon emission process by combining time-dependent perturbation theory and the transmission line modelling method. From the theory, both intersubband transitions and interband transitions can be modelled by the Q-TLM method. This method adopts topological structures to describe the dynamic photon–electron interaction processes, and has been successfully employed to model quantum well devices in the near-infrared wavelength range [28]. This approach is adapted from transmission line matrix (TLM) theory, which was initially used to solve field equations and describe microwave propagation in microwave circuits [29-30]. The THz QCL operates at the frequencies between microwave and infrared spectral regions and its active region consists of a cascade of quantum wells. We show here, for the first time, that Q-TLM is also an effective method for dynamic modelling of THz devices.

Our model describes QCLs using parallel quantum-cascade transmission line modelling units and is used to predict the transients in output power after switch-on, and to simulate both its current–power characteristics and emission spectrum in steady-state. The predicted lasing-threshold current density and variation of emission spectrum with changing injection current are shown to agree well with experimental measurements. A Q-TLM model is also developed for a THz QCL incorporating a photonic lattice (PL) patterned on the laser ridge [31], which is important for the development of single mode THz QCLs required for local oscillators [32] and THz sensing applications [33]. The simulated effect of the PL structure on the QCL emission spectrum, including the suppression of side modes, is in good agreement with experiments.

This paper is organized as follows. Section 2 introduces the new Q-TLM model for a THz QCL following calculation of its

band structure. In Section 3, the model is used to analyze the output properties of a THz QCL, including its current–power characteristics and the variation of the emission spectrum with injected current. These predictions are then compared with experimental measurement results obtained from an exemplar THz QCL. In Section 4, a THz QCL incorporating an integrated PL is modelled using the Q-TLM method. The effects of the PL grating structure on the output spectrum of the QCL are studied both theoretically and experimentally. Finally, conclusions are given in Section 5.

## II. THEORETICAL MODEL

### A. Band structure

The THz QCL used in this study is based on a nine-well design [34] with GaAs quantum wells and  $\text{Al}_{0.18}\text{Ga}_{0.82}\text{As}$  barriers. This design is based on alternating photon and longitudinal optical (LO) phonon-assisted transitions between quasi-minibands. The active region layer thicknesses of one period in Å are **38/108/5/126/10/129/19/113/29/91/29/82/29/68/29/163/29/142**, where the bold numbers refer to the barriers and the underlined layer denotes the Si-doped GaAs layer with doping density  $3.0 \times 10^{16} \text{ cm}^{-3}$ .

The energies and corresponding wave-functions for electronic states within the structure were computed using a parabolic effective-mass solution to the Schrödinger equation [35], using material parameters from [35-36]. Figure 1 shows the conduction band potential and the squared amplitude of the envelope wave functions in two periods of the active region under an external electric field of 5.2kV/cm. The lasing transition takes place from state 3 or state 2 to the miniband  $mn'$  whereas the LO-phonon assisted transition takes place from the miniband  $mn$  to state 2 or state 1.

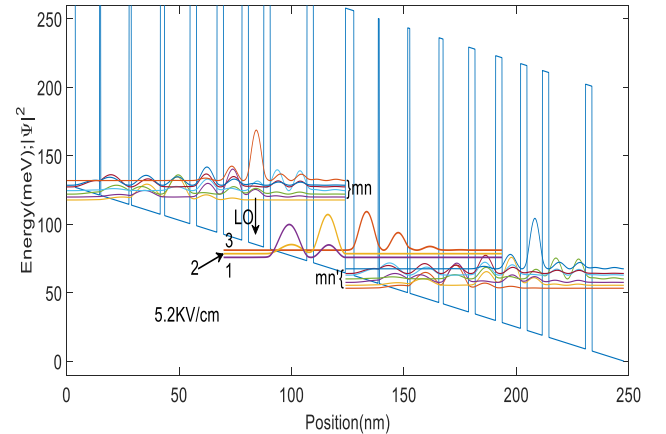


Fig. 1 Band structure and squared envelope wave functions obtained by solving Schrodinger equations.

### B. Q-TLM Model of THz quantum cascade laser

In the following section, the Q-TLM method is adopted to establish a new model for a THz QCL. The basic structure for the Q-TLM model of THz QCLs is the Q-TLM unit, which is used to describe the dynamic photon emission process during

the electronic intersubband transitions at a given wave vector. As QCLs contain several subbands, photons can be generated from the different intersubband transitions. Several parallel Q-TLM units are employed to constitute the quantum cascade transmission line modelling unit (QC-TLM unit), which is used to model the main lasing transitions at the given vector. Furthermore, QC-TLM units are combined in parallel to describe the photon emission over a range of in-plane electron wave vectors. The optical processes, such as the stimulated emission and the spontaneous emission are described based on the parallel QC-TLM units.

Figure 2 shows the structure of one Q-TLM unit. Each Q-TLM unit includes a resonant two-level RLC system (consisting of a resistor, capacitor and inductor with characteristic admittances of  $Y_R$ ,  $Y_C$  and  $Y_L$  respectively) as well as a weight coefficient  $K$ . At high frequencies, the capacitors and inductors are described by open-circuit and short-circuit transmission lines, respectively [37].

Based on the Heisenberg's uncertainty principle, the finite lifetime of an excited state lead to the uncertainty in the energy of electron transition, which results in a finite Lorentzian linewidth in frequency. The Lorentzian linewidth in frequency is given by:

$$H_1(\omega) = \frac{1}{\pi \hbar} \frac{\gamma / 2}{(\omega - 2\pi f_{BA})^2 + (\gamma / 2)^2} \quad (1)$$

where  $\gamma$  is the homogeneous linewidth broadening,  $\hbar$  is the Plank constant  $h$  divided by  $2\pi$ ,  $f_{BA}$  is determined by the frequency of the generated photon through intersubband electron transitions in the QCL, which can be expressed as:

$$f_{BA} = (E_B - E_A) / h \quad (2)$$

where  $E_B$  and  $E_A$  are the energies for higher energy state B and lower energy state. The frequency response of the two-level RLC network in the Q-TLM unit can be expressed as:

$$H(\omega) = \frac{\omega_0}{2Q} \frac{\omega_0 / 2Q}{(\omega - \omega_0)^2 + (\omega_0 / 2Q)^2} \quad (3)$$

where,  $Q$  is the quality factor of the RLC system,  $\omega_0 = 2\pi f_{BA}$  is the resonant angular frequency. In order to describe the homogeneous linewidth broadening using the RLC system, by comparing Eq. (1) and Eq. (3), it can be found that:

$$H_1(\omega) = \frac{2}{\pi \gamma \hbar} H(\omega) \quad (4)$$

The resistance value is 1 and the characteristic admittance expressions of the inductor and capacitor in the Q-TLM unit are [32]:

$$Y_L = Q \tan(\pi \Delta T f_{BA}) \quad (5)$$

$$Y_C = Q / \tan(\pi \Delta T f_{BA}) \quad (6)$$

$$Q = \frac{2\pi f_{BA}}{\gamma} \quad (7)$$

where  $\Delta T$  is the optical field propagation time along the link transmission line and it is the smallest time interval in the modelling and determines the resolution of the electric field in the time domain. The sampling frequency can be defined as:

$$f_{sam} = 1 / \Delta T \quad (8)$$

The weighting coefficient in the Q-TLM unit describes the electron-transition possibility between two conduction subbands at a certain wave vector, and can be expressed as [35]:

$$K = \frac{4\pi G_0}{V \hbar} |H'_{BA}|^2 (F_B - F_A) \quad (9)$$

where  $H'_{BA}$  is the matrix element for the transition,  $F_B$  and  $F_A$  are the Fermi-Dirac distribution function for the higher energy state B and lower energy state A,  $G_0$  is the magnitude coefficient and  $V$  is the crystal volume. In Fig. 2,  $E_{in}(z, t)$  and  $E_{out}(z, t)$  denote the input electric field and the output electric field, respectively.

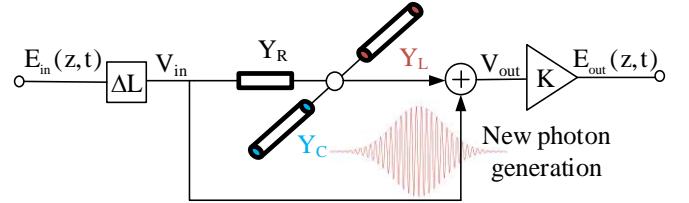


Fig. 2 Structure of quantum transmission line modelling (Q-TLM) unit. The resonant RLC system ( $Y_R$ ,  $Y_C$  and  $Y_L$ ) describes the photon generation process and the weighting coefficient ( $K$ ) expresses the probability of the photon generation.

One Q-TLM unit is the basic unit for the model of THz QCL. The specific voltage propagation process in one Q-TLM unit is shown in Fig. 3.

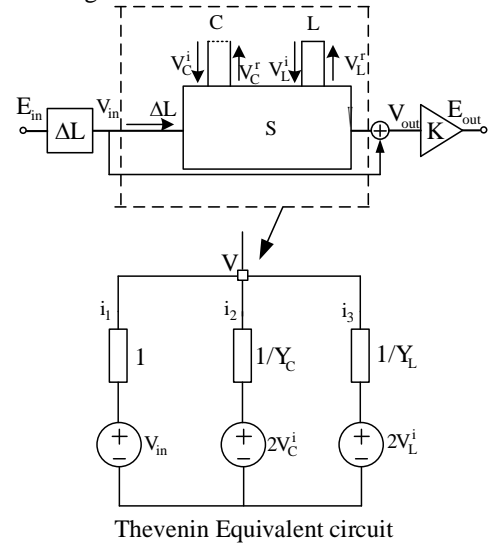


Fig. 3 The voltage propagation process in one Q-TLM unit and its Thevenin equivalent circuit.

The input transmission line with the length  $\Delta L$  is used to model the resistor and the open and short stub transmission lines with length  $\Delta L / 2$  are used to represent the capacitor and inductor. Based on the transmission line theory, the corresponding Thevenin equivalent circuit can be obtained (as shown in Fig. 3). The node voltage  $V$  can be expressed as [37]

$$V = \frac{1}{Y} (i_1 + i_2 + i_3) = \frac{1}{Y} (V_{in} + 2Y_C V_C^i + 2Y_L V_L^i) \quad (10)$$

$$Y = 1 + Y_C + Y_L \quad (11)$$

where,  $V_{in}$  is the input voltage,  $V_C^i$  and  $V_L^i$  are the incident voltages of the capacitive and inductive stub lines, respectively,  $Y_C$  and  $Y_L$  are the characteristic admittance of the inductor and

capacitor in the Q-TLM unit, which are given in Eqs.(5)and(6). The output electric field can be obtained by

$$E_{\text{out}} = KV_{\text{out}} = K(V + V_{\text{in}}) \quad (12)$$

where,  $K$  is the weight coefficient (as shown in Eq. (9)) and the input voltage  $V_{\text{in}}$  can be expressed in terms of the electric field in the link transmission line as  $V_{\text{in}} = E_{\text{in}}\Delta L$ . During the time interval  $\Delta T$ , the input voltage propagates along the link transmission line and arrives at the scattering node and at the same period, the reflected voltages of the capacitor and inductor propagate to the end of the stub transmission lines and back again at the scattering node. After one iteration, the reflected voltage will return and become the new incident voltage [37].

Since QCLs contain several subbands, photons can be generated through a number of different transitions. Several Q-TLM units are therefore used, in parallel, to describe the photon emission due to each intersubband transition. Here we refer to the parallel Q-TLM units as quantum cascade transmission line modelling (QC-TLM) units. Figure 4 shows the structure of one such unit, taking into account three electron transition processes from state 3 to state 2 ( $3 \rightarrow 2$ ), from state 3 to state mn ( $3 \rightarrow mn$ ) and from state 2 to state mn ( $2 \rightarrow mn$ ). The number of Q-TLM units in a QC-TLM unit is determined by the main lasing transitions in the THz QCL under consideration.

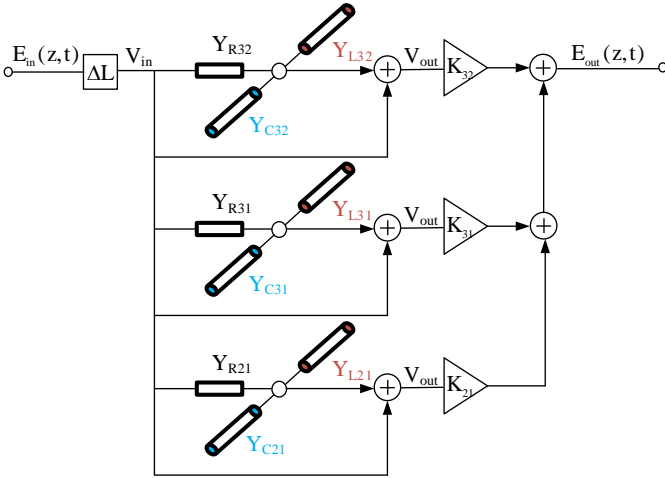


Fig. 4 Structure of quantum cascade transmission line modelling (QC-TLM) unit. Here three Q-TLM units constitute the QC-TLM unit, which corresponds to the photon emissions from the electron transitions from state 3 to state 2, state 3 to state mn and state 2 to state mn between the conduction subband.

Next, QC-TLM units are combined in parallel to describe the photon emissions over a range of in-plane electron wave vectors. These parallel units are then used to form topological modules that describe the optical process either stimulated emission or spontaneous emission processes in the THz QCL. Fig. 5a and 5b show the structures of the scattering module (SM) and spontaneous emission module (SEM), respectively. The SM (as seen in Fig. 5a) consists of parallel QC-TLM units (describing stimulated emission at a range of electron wave vectors) and gain coefficient  $G$ . The spontaneous emission

module (Fig. 5b) consists of a spontaneous emission source, parallel QC-TLM units (describing spontaneous emission at a range of electron wave-vectors) and a spontaneous emission coupling factor  $\beta$ . The gain coefficient  $G$  can be derived from the time-dependent perturbation theory and can be defined as [38]

$$G = \frac{\Gamma q^2}{\pi \hbar n_r c \epsilon_0 m_0^2 L_z \gamma} \quad (13)$$

where,  $\Gamma$  is the optical confinement factor for the entire active region,  $q$  is the magnitude of the electron charge,  $n_r$  and  $\epsilon_0$  are the refractive index and the permittivity in free space, respectively,  $c$  is the speed of light in free space,  $m_0$  is the electron mass in free space,  $L_z$  is the width of the quantum well in which the main lasing transition occurs. Based on Eq. (9), the weighting coefficient of the Q-TLM unit in the scattering module can be expressed as:

$$K_{ij} = f_{ij} |P_{ij}|^2 [F_i(E) - F_j(E)] \quad (14)$$

where  $f_{ij} = (E_i^c - E_j^c)/\hbar$ ,  $E_i^c$  and  $E_j^c$  are the discrete confined energies in the  $i^{\text{th}}$  and  $j^{\text{th}}$  conduction subband ( $E_i^c > E_j^c$ ),  $|P_{ij}|^2$  is the momentum matrix element and  $F_i(E)$  and  $F_j(E)$  are the Fermi-Dirac distribution functions for the  $i^{\text{th}}$  and  $j^{\text{th}}$  conduction subband. The spontaneous emission source  $S_{\text{ASE}}$  is given by [27]:

$$S_{\text{ASE}} = \begin{cases} \frac{E_0}{q\Delta L} & \text{for } t = nT_0, n = 0, 1, 2, \dots \\ 0 & \text{for } (n-1)T_0 < t < nT_0, n = 1, 2, \dots \end{cases} \quad (15)$$

where  $E_0$  is the average energy of a spontaneously-emitted photon,  $T_0$  is the excited state lifetime in the spontaneous emission, and  $\Delta L$  is the length of the link transmission line ( $\Delta L/2$  is the length of each stub transmission line representing the capacitor and inductor). The weighting coefficient of the QC-TLM unit in the spontaneous emission module is given as:

$$K'_{ij} = \beta f_{ij}^3 |P_{ij}|^2 F_i(E) [1 - F_j(E)] / \left(1 - \frac{\exp\left[\frac{E - (E_i^c - E_j^c)}{k_B T}\right]}{K_B T}\right) \quad (16)$$

where  $\beta$  is the spontaneous emission coefficient. The weight coefficients of the QC-TLM units in the scattering module and spontaneous module are derived from the optical transitions using Fermi's Golden rule. Quasi-fermi levels were employed for the higher energy state and the lower energy state and both of them are dependent on carrier density. Specifically, the bisection method is used to calculate the quasi-fermi levels in the simulation, respectively.

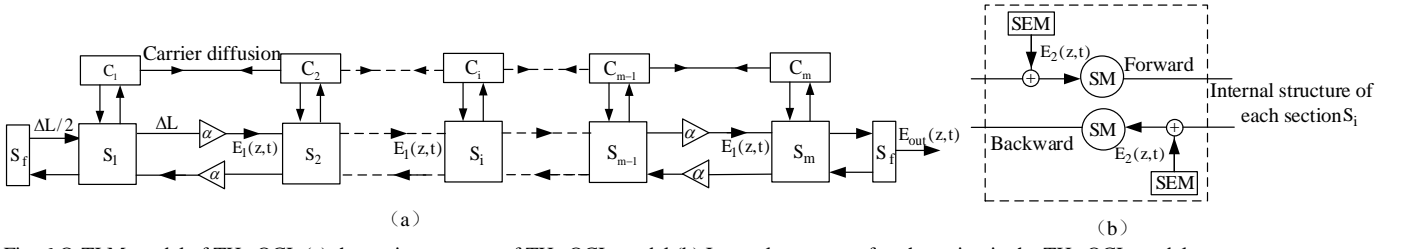


Fig. 6 Q-TLM model of THz QCL (a) the cavity structure of THz QCL model (b) Internal structure of each section in the THz QCL model

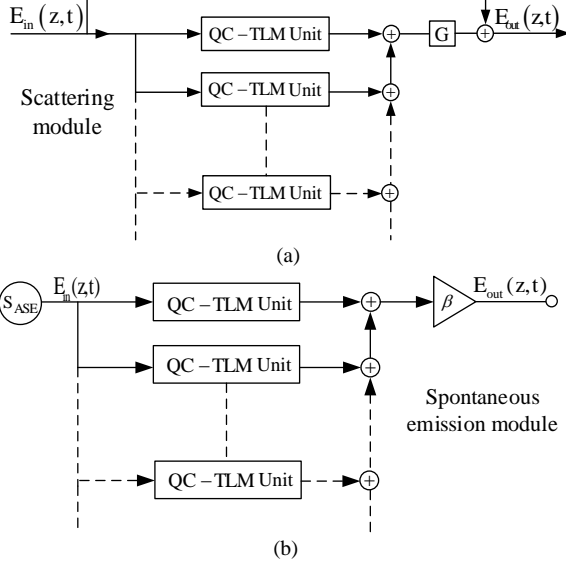


Fig. 5 Modelling optical processes in THz QCL based on Q-TLM (a) structure of scattering module for describing stimulated emission process in THz QCL (b) structure of spontaneous emission module for describing spontaneous emission process in THz QCL

The complete Q-TLM model for a THz QCL is constructed using the modules described above. In this model, the laser cavity is divided into  $m$  small sections (from  $S_1$  to  $S_m$ ) along the longitudinal direction, as shown in Fig. 6a. The number of sections  $m$  is determined by  $L/\Delta L$ , where  $L$  is the cavity length. Section  $S_f$  in Fig. 6a is the facet model, which is used to describe the Fresnel reflection and transmission at both of the laser facets [39]. Figure 6b shows the internal structure of each section, which includes the forward and backward SM and SEM modules (as shown in Fig. 5).  $\alpha$  is the transmission coefficient, which is used to describe the THz wave propagation loss.

In Fig. 6a,  $C_i$  denotes the carrier density of the main states in the  $i$ th section of the Q-TLM model, including the carrier densities for the upper lasing level, the lower lasing level and the miniband state. The variation of  $C_i$  is given as [15]

$$\frac{dn_3}{dt} = \eta_3 \frac{J}{qD} - \frac{n_3}{\tau_3} - \frac{\Gamma}{q\Delta V} \frac{V_{in}}{Z_p} \quad (17)$$

$$\frac{dn_2}{dt} = \eta_2 \frac{n_3}{\tau_{32}} - \frac{n_2}{\tau_2} + \frac{\Gamma}{q\Delta V} \frac{V_{in}}{Z_p} \quad (18)$$

$$\frac{dn_1}{dt} = \eta_1 \frac{n_3}{\tau_{31}} + \frac{n_2}{\tau_{21}} - \frac{n_1}{\tau_1} \quad (19)$$

where,  $n_j$  ( $j=1,2,3$ ) is the carrier density in level  $j$ ,  $\eta_j$  is the injection efficiency in level  $j$ ,  $J$  is the injection current density,  $D$  is the thickness of the active region,  $1/\tau_j$  is the total scattering rate for electrons leaving level  $j$ , which is calculated by Fermi Golden Rule,  $\Delta V$  is the volume of each section in the cavity model,  $Z_p$  is the transverse wave impedance, which is given as  $(\mu/\epsilon)^{1/2}$ , where  $\mu$  and  $\epsilon$  are the permeability and permittivity of the bulk material, respectively, and  $V_{in}$  is the input voltage of the QC-TLM unit in the scattering module.

### III. THEORETICAL AND EXPERIMENTAL ANALYSIS OF THZ QUANTUM CASCADE LASER

#### A. Theoretical simulation based on the Q-TLM model

When Q-TLM is used to model the THz QCL, it is important for us to calculate the band structure and wavefunctions for obtaining the parameters related to the basic Q-TLM unit. As mentioned above, the frequency  $f_{BA}$  in the characteristic admittance expressions for the capacitor and inductor in one Q-TLM unit is determined by the generated photon through intersubband electron transitions; it can be obtained by calculating the band structure of the cascade quantum wells. In the simulation, the band structure is varied with the bias current [40] and the sampling frequency  $f_{sam}$  needs to satisfy the Nyquist-Shannon sampling theorem; The optical confinement factor and the spontaneous emission coefficient are chosen based on the empirical values.

In the following, the proposed Q-TLM model is used to analyze the output properties of an exemplar GaAs/AlGaAs THz QCL in the time and frequency domains. The active region of the THz QCL consists of nine GaAs quantum wells in one period with 115 periods being repeated along the growth direction. Section 2.1 has shown the composition of wells and barriers in one period as well as the calculated conduction band and wave functions. Other parameters used in the simulation are given in Tab. 1 and Ref. [35].

Figure 7 shows the output optical power calculated as a function of injected current at a temperature 30K using the Q-TLM model for a THz QCL device with cavity length 1.8 mm. In the Q-TLM model, the temperature and carrier density influence the weight coefficient  $K$  of each QC-TLM unit (referring to the above Eqs. (14) and (16)). The output optical

power is obtained by converting from the output electric field  $E_{\text{out}}(z, t)$  (shown in Fig. 6(a)). Also, it should be noted that in this case the output power value at each injected current is obtained when the output reaches the steady state. It can be found that the maximum calculated output power is 18.6mW at the injected current 1200mA. The simulation results indicate the threshold current of the 1.8mm-long THz QCL is  $I_{\text{th}}=350\text{mA}$ , which corresponds to a current density  $129.6\text{A}/\text{cm}^2$ .

TABLE 1 SIMULATION PARAMETERS OF THz QCL

Symbol	Description	Value
$f_{\text{sam}}$	Sampling frequency	$4.27 \times 10^{14}\text{Hz}$
$\Delta L$	Length of link transmission line	180nm
$\Gamma$	Optical confinement factor	0.3
$\beta$	Spontaneous emission coefficient	0.01
$\gamma$	Linewidth broadening of photon emission	$2.37 \times 10^{12}\text{rad/s}$
$\alpha$	Transmission coefficient in each section	0.9999/m
$n_r$	Refractive index	3.9
$\Delta F$	Transform resolution	427MHz
$\Delta T$	Time step	2.34fs
L	Length of THz-QCL	1.8mm
D	Thickness of active region	14 $\mu\text{m}$
W	Width of active region	150 $\mu\text{m}$

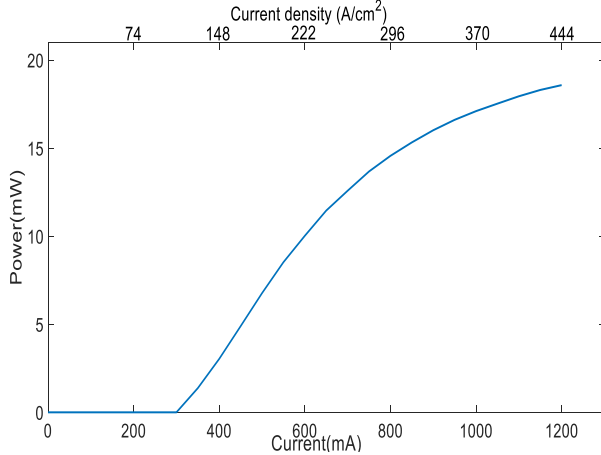


Fig. 7 Output power versus injected current of a 1.8mm long THz QCL. The simulation results are obtained based on the proposed Q-TLM model of THz QCL in Section 2.

Figure 8a shows the turn-on transient (output power plotted in the time-domain) of the THz QCL obtained from the Q-TLM model at a temperature of 30K. In this simulation, we have assumed an injected current of 1000mA (current density  $370.4\text{kA}/\text{cm}^2$ ) at the initial time  $t=0$ . It can be seen that the turn-on transient is characterized by a period of oscillation for  $t=0\sim 1\text{ns}$  before attaining steady state, after which the calculated average output power is 17.1mW. These initial oscillations can be explained by the dynamic carrier transport processes occurring in the active region. Furthermore, for the output in the steady stage, there exists amplitude oscillation which is due to the beating in the multi-mode lasing. The simulation result is similar with the phase-resolved

experimentally measured THz QCL field shown in Refs. [41-42].

Using our model it is also possible to obtain the output power spectral density of the THz QCL, by applying a Fast Fourier Transform (FFT) to the steady state output electric field in the time-domain. This is shown in Fig. 8b, which predicts the central frequency of the output power spectral density to be 3.44THz. It is also predicted that the THz QCL exhibits multi-mode lasing behavior for this injected current of 1000mA, which is much larger than the threshold current ( $=2.86 I_{\text{th}}$ ). Such behavior is typical of that observed experimentally in THz QCL devices.

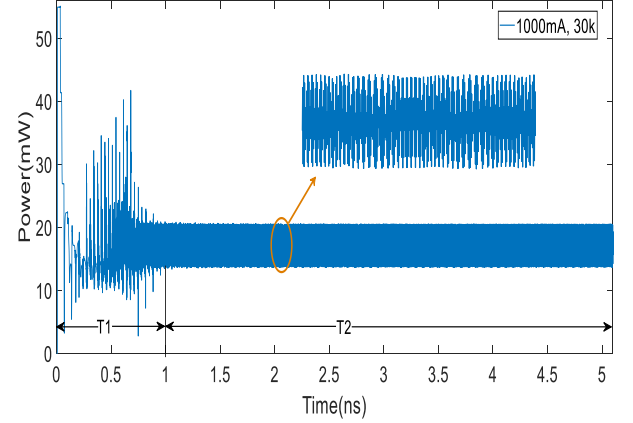


Fig. 8a Turn-on transient of THz QCL obtained based on the Q-TLM model.

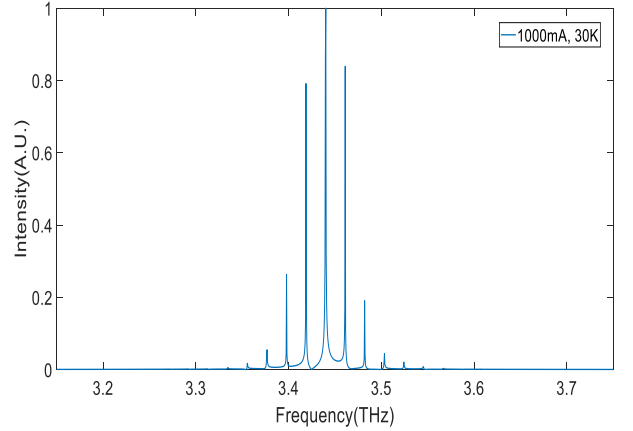


Fig. 8b Output power spectral density of THz QCL at the steady stage obtained based on the proposed Q-TLM model for an injection current of 1000 mA.

In order to further explore the spectral emission predicted by our Q-TLM model, the output spectra were similarly calculated for a range of injection currents from 400mA to 1200mA, as shown in Fig. 9. At an injection current of 400mA ( $=1.14 I_{\text{th}}$ ) the predicted output spectrum is dominated by a single lasing mode at 3.291THz, which corresponds to the energy bandgap from state 3 to the mini-band. Multi-mode emission appears when the injected current exceeds 600mA ( $222.2\text{kA}/\text{cm}^2$ ). It can be found that the frequency interval between the adjacent modes is 0.021THz, which agrees with the Fabry-Perot mode spacing determined by the length of QCL cavity and the refractive index of the active region. Furthermore it is found that as the injected current increases, the output spectrum shifts to higher frequency, a behavior that is typical in QCLs due to the Stark shift of the intersubband gain curve. The side mode

suppression ratios (SMSR) for each of the injection currents in the range 400-1200 mA shown in Fig. 9 are calculated to be 0.1, 0.784, 0.970, 0.840 and 0.741, respectively.

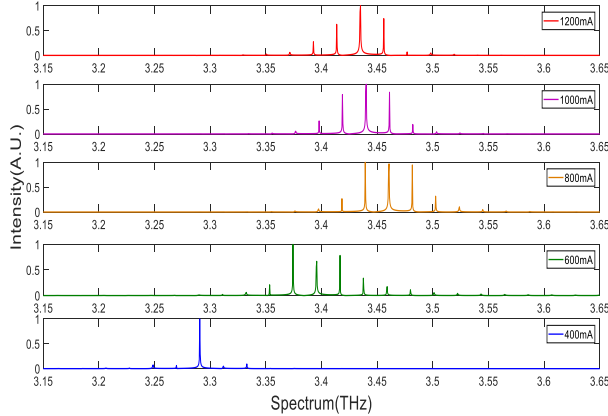


Fig. 9 The output spectra of THz QCL at a range of bias currents (from 400mA to 1200mA) obtained by the Q-TLM simulation.

## B. Experimental analysis and comparison

To validate the predictions of our model, a comparative QCL device was fabricated with the same structure and material composition as the above simulated THz QCL. The  $14\mu\text{m}$  thick active region stack, comprising 115 periods of the nine well structure shown in Section 2.1, was grown by molecular beam epitaxy on a semi-insulating GaAs substrate. The active region is embedded between a top (50nm thick) and bottom (700nm thick)  $n^+$ -GaAs layer, with Si doping levels of  $5 \times 10^{18} \text{ cm}^{-3}$  and  $2 \times 10^{18} \text{ cm}^{-3}$ , respectively. Following growth, the structure was processed into a surface plasmon ridge waveguide with a width  $150\mu\text{m}$ . A 1.8mm long cavity was formed by mechanical cleaving, which was then soldered to a copper submount using indium. The device was cooled using a continuous-flow helium cryostat and operated in continuous wave mode at a heat sink temperature of 30K. The output power of the QCL was measured using a helium-cooled Ge:Ga bolometric detector, which was calibrated using a Thomas-Keating THz photoacoustic absolute-power meter. Emission spectra of the THz QCL were obtained using a Bruker Fourier Transform Infrared (FTIR) spectrometer with spectral resolution of 7.5 GHz.

Figure 10 shows the experimentally measured output power versus the injected current at an operating temperature of 30K. As can be seen, the experimental current-power relationship agrees remarkably well with the theoretical predictions of our model shown in Fig. 7. Specifically, the measured threshold current is found to be  $135.2 \text{ A/cm}^2$ , which is very close to the  $129.6 \text{ A/cm}^2$  threshold current predicted by the Q-TLM model. Furthermore, the maximum output power was measured to be 18.7mW, which is close to the predicted value of 17.1mW.

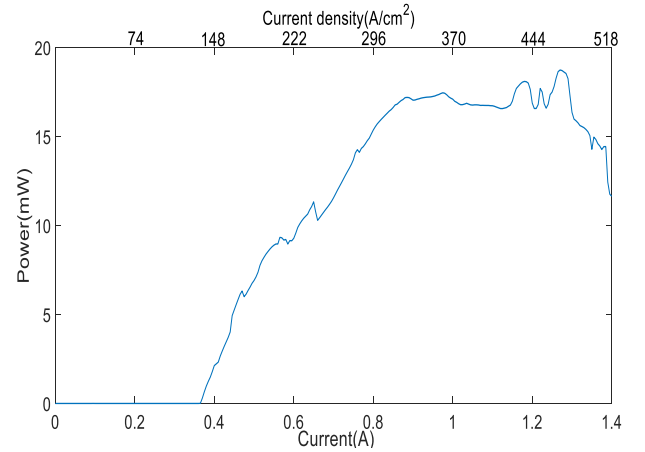


Fig. 10 Experimental measured emitted power versus the injected current at the sink temperature 30K in the continuous wave mode

The emission spectra measured for injection currents in the range 400-1200mA are shown in Fig. 11. As can be seen, with an injection current of 400mA the device is found to lase predominantly at a frequency of 3.295THz, which is very close to the simulated emission frequency of 3.291THz. Furthermore, as the injection current increases the emission spectrum is seen to shift to higher frequencies and also broaden, with lasing on multiple longitudinal modes being observed when the injection current is greater than  $\sim 600\text{mA}$ . These experimental results are in very good agreement with the theoretical predictions shown in Fig. 9. Also, it can be observed that the peaks of the measured emission spectrum are broader than those in the simulation because its limited by the FTIR resolution.

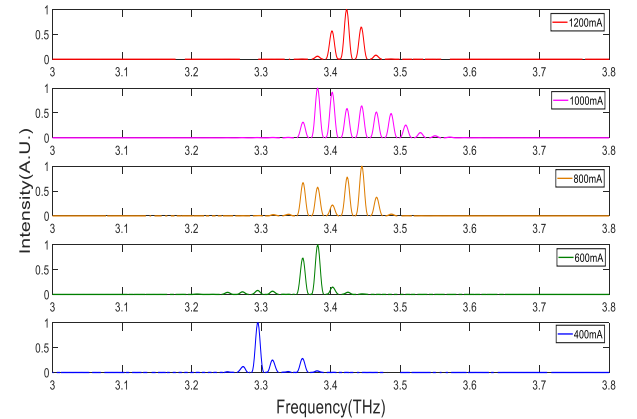


Fig. 11 Emission spectra of THz QCL at a range of bias currents at the temperature 30K. The applied bias currents of the THz QCL are 400mA, 600mA, 800mA, 1000mA and 1200mA, respectively. The results are measured using FTIR with the minimum resolution 7.5GHz

## IV. THEORETICAL AND EXPERIMENTAL ANALYSIS OF THz QCL WITH PHOTONIC LATTICE

### A. Modelling THz QCL with the photonic lattice structure based on Q-TLM

In recent years there has been growing interest in the incorporation of photonic lattice (PL) structures in QCL waveguides for spectral control[31, 42]. In particular, single mode emission is highly desirable for a range of applications

including trace gas sensing, heterodyne mixing and laser feedback interferometry. In this section, the proposed Q-TLM method is further used to analyse the output performance of a THz-QCL incorporating a PL patterned on the laser ridge. The structure of the PL-QCL consists of waveguide sections of length  $L_m$  with cladding metal (metallised) interleaved with sections of length  $L_g$  without cladding metal (unmetallised). The PL grating comprises a finite number of such periods, with grating pitch  $\Lambda = L_m + L_g$ , which are located in the center of the laser ridge as depicted in Fig. 12

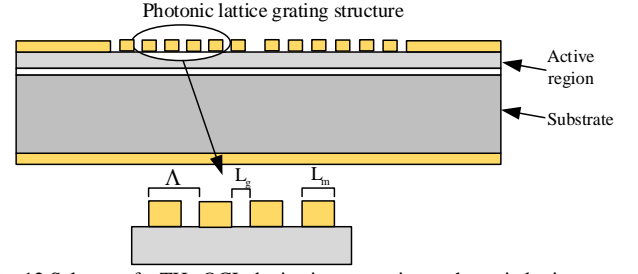


Fig. 12 Scheme of a THz QCL device incorporating a photonic lattice structure (PL-QCL). One grating pitch  $\Lambda$  consists of a metallised section with length  $L_m$  and an unmetallised section with length  $L_g$ .

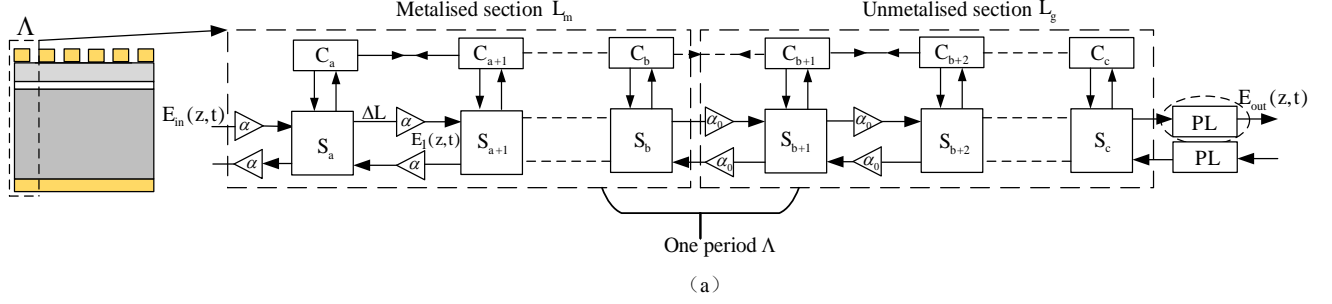


Figure13 Q-TLM model for the THz PL-QCL (a) the model structure for THz QCL with one period length (b) the internal structure of PL

Figure 13 shows the Q-TLM model for the THz PL-QCL with one-period ( $\Lambda$ ) length. The different transmission coefficients  $\alpha$  and  $\alpha_0$  are used to describe the THz wave transmission loss in the metallised section and the unmetallised section, respectively. The internal structure for each section  $S$  and the variation of carrier density  $C$  have been shown in Fig. 6 and Eqs. 17-19. The transmission line structure of PL in Fig. 13a are shown in Fig. 13b.

The Q-TLM model for THz QCL describes the varying temporal THz field along the cavity by modelling the electron-photon interaction process and the optical field propagation process. Both the two processes have been modelled by the varying impedances (capacitor and inductor). In order to model the effects induced by the photonic lattice structure, the transmission line structure of PL (shown in Fig. 13b) is connected in series in each period of the photonic lattice structure. The transmission line structure of PL has brought the periodic changes in the equivalent impedance. In Fig. 13b, the resistor value is 1 and the expressions for the inductor and capacitor are defined as:

$$Y_L = Q_{pl} \tan(\pi \Delta T f_{PL}) \quad (20)$$

$$Y_C = Q_{pl} / \tan(\pi \Delta T f_{PL}) \quad (21)$$

where  $\Delta T$  is the optical field propagation time along the link transmission line, the frequency  $f_{PL}$  is determined by the Bragg frequency  $f_{BR}$  of the PL, which is given as:

$$f_{PL} = f_{BR} = \frac{c l_{pl}}{2 n_{eff} \Lambda} \quad (22)$$

where  $n_{eff}$  is the effective refractive index and  $l_{pl}$  is the PL order ( $l_{pl} = 1$  for the first order). The quality factor  $Q_{pl}$  is determined by

$$Q_{pl} = \frac{2\pi f_{BR}}{\Delta f_{BR}} \quad (23)$$

where  $\Delta f_{BR}$  is the bandwidth of the PL. The input port of the PL structure in Fig. 13b is linked to the output port of the scattering module (shown in Fig. 5a of Section 2).

## B. Q-TLM and experimental analysis of PL-QCL

In the following, the Q-TLM method is used to simulate the effect of the integrated PL on the emission spectra of a THz QCL device. These predications are then compared to experimental measurements obtained from an exemplar PL-QCL device. The PL structure analysed here consists of 12 periods of grating pitch, which is situated in the center of the waveguide along the longitudinal direction. One period with the length  $\Lambda = 13 \mu\text{m}$  includes the unmetallised section with the length  $L_g = 4 \mu\text{m}$  and the metallized section with the length  $L_m = 9 \mu\text{m}$ ; a single central ‘phase shift’ section with the length  $8 \mu\text{m}$  is also included in the PL structure.

Figure 14 shows the steady-state output spectrum of the PL-QCL obtained by the Q-TLM method for an injection current of 1000mA and an operating temperature of 30K. The propagation coefficient for the unmetallised section used in the simulation was 0.9998. In this case it is found that the emission

spectrum is dominated by a single lasing mode at 3.501THz, which represents a blue shift compared with the output spectrum predicted for the case without the PL structure (Fig. 8b). Further comparison of Fig. 14 and Fig. 8b shows that the PL structure can effectively suppress the side modes and contribute to single mode emission. From the simulation results, the SMSR of the THz QCL output spectra with and without the PL structure are 0.05 and 0.840, respectively.

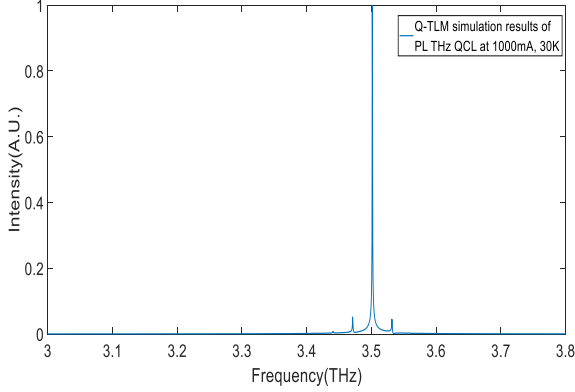


Fig. 14 Steady output spectrum of PL-QCL obtained based on Q-TLM model at the injected current 1000mA and temperature 30K.

A THz QCL device with the same PL structure as described above was then fabricated by focused-ion beam milling the plasmonic cladding metallic layer of the THz QCL ridge mentioned in Section 3. Figures 15a and 15b show the SEM pictures of the waveguide before and after the PL was defined. Figure 16 shows the measured emission spectrum of the PL-QCL obtained with an injection current of 1000mA and at an operating temperature 30K. Lasing on a single longitudinal mode at 3.514THz is observed, in good agreement with the frequency predicted from the Q-TLM model. Indeed, by comparing Fig. 14 with Fig. 16, it can be seen that the simulated output spectrum of the PL-QCL is in good agreement with the experimentally measured spectrum. The results confirm that the Q-TLM model can effectively simulate the effects of the PL structure on the output spectrum of a THz QCL.

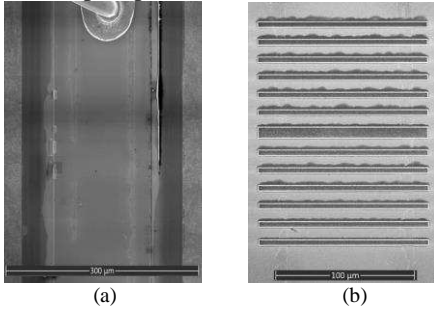


Fig. 15 SEM pictures of the top of the waveguide of THz QCL (a) without the photonic lattice grating structure (b) with the photonic lattice grating structure

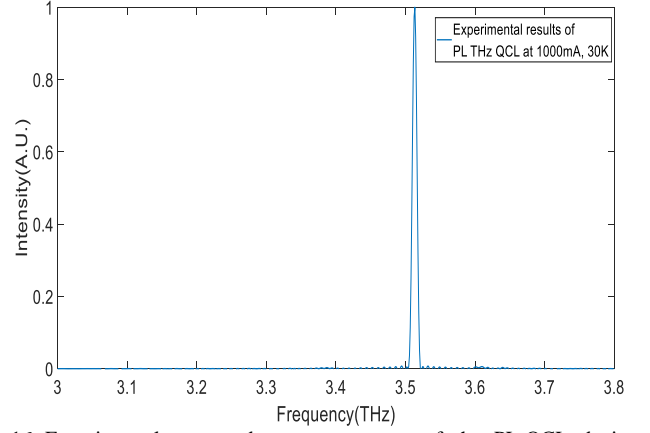


Fig. 16 Experimental measured output spectrum of the PL-QCL device obtained with an injection current of 1000mA and at an operating temperature 30K.

## V. CONCLUSIONS

In this paper, we have established a new theoretical approach for modelling the optoelectronic properties of a THz QCL based on a Q-TLM method. In this model, topological parallel QC-TLM units are used to describe the optical processes in the THz QCL. We have used the newly proposed model to simulate the current-power characteristics of a QCL device as well as its emission spectrum. By comparison with experimental measurements of a THz QCL device we have confirmed that the Q-TLM model can accurately predict the lasing threshold current density, emitted power and also the variation of the emission spectrum with changing injection current. We have furthermore adopted the Q-TLM method to model a THz QCL device incorporating a photonic lattice patterned on the laser ridge. The effects of PL structure on the output spectrum of the THz QCL have been studied and simulation results are found to be in good agreement with experimental measurements. The proposed Q-TLM method provides a promising tool for the design and dynamic analysis of THz QCLs in the time and frequency domains.

## REFERENCES

- [1] R. Köhler, A. Tredicucci, F. Beltram, H. E. Beere, E. H. Linfield, A. G. Davies, D. A. Ritchie, R. C. Iotti and F. Rossi, "Terahertz semiconductor-heterostructure laser," *Nature*, vol. 417, pp. 156-159, 2002.
- [2] L. Li, L. Chen, J. Zhu, J. Freeman, P. Dean, A. Valavanis, A. G. Davies, and E. H. Linfield, "Terahertz quantum cascade lasers with >1 W output powers," *Electron. Lett.*, vol. 50, pp. 309-311, 2014.
- [3] B. J. Williams, "Terahertz quantum-cascade lasers," *Nature*, vol. 1, pp. 517-525, 2007.
- [4] M. S. Vitiello, G. Scalari, B. J. Williams, and P. D. Natale, "Quantum cascade lasers: 20 years of challenges," *Opt. Express*, vol. 23, pp. 5167-5182, 2015.
- [5] B. J. Williams, H. Callebaut, S. Kumar, Q. Hu, and J. Reno, "3.4-thz quantum cascade laser based on longitudinal-optical-phonon scattering for depopulation," *Appl. Phys. Lett.*, vol. 82, pp. 1015-1017, 2003.
- [6] D. Turčinková, G. Scalari, F. Castellano, M. I. Amanti, M. Beck, and J. Faist, "Ultra-broadband heterogeneous quantum cascade laser emitting from 2.2 to 3.2 THz," *Appl. Phys. Lett.*, vol. 99, pp. 191104, 2011.
- [7] F. Wang, K. Maussang, S. Moudjji, R. Colombelli, J. R. Freeman, I. Kundu, L. Li, E. H. Linfield, A. G. Davies, J. Mangeney, J. Tignon and S. S. Dhillon, "Generating ultrafast pulses of light from quantum cascade lasers," *Optica*, vol. 2, pp. 944-949, 2015.

- [8] P. Dean, A. Valavanis, J. Keeley, K. Bertling, Y. L. Lim, R. Alhathlool, S. Chowdhury, T. Taimre, H. L. Li, D. Indjin, S. J. Wilson, A. D. Rakić, E. H. Linfield and A. G. Davies, "Coherent three-dimensional terahertz imaging through self-mixing in a quantum cascade laser," *Appl. Phys. Lett.*, vol. 103, pp. 181112, 2013.
- [9] A. G. Davies, A. D. Burnett, W. H. Fan, E. H. Linfield and J. E. Cunningham, "Terahertz spectroscopy of explosives and drugs," *Mater. Today*, vol. 11, pp. 18-26, 2008.
- [10] Z. Chen, Z. Y. Tan, Y. J. Han, R. Zhang, X. G. Guo, H. Li, J. C. Cao and H. C. Liu, "Wireless communication demonstration at 4.1 THz using quantum cascade laser and quantum well photodetector" *Electron. Lett.*, vol. 47, pp. 1002-1004, 2011.
- [11] J. R. Freeman, L. Ponnampalam, H. Shams, R. A. Mohandas, C. C. Renaud, P. Dean, H. L. Li, A. G. Davies, A. J. Seeds and E. H. Linfield, "Injection locking of a terahertz quantum cascade laser to a telecommunications wavelength frequency comb," *Optica*, vol. 4, pp. 1059-1064, 2017.
- [12] D. Indjin, P. Harrison, R. W. Kelsall and Z. Ikonic, "Self-consistent scattering theory of transport and output characteristics of quantum cascade lasers," *J. Appl. Phys.*, vol. 91, pp. 9019-9026, 2002.
- [13] F. Compagnone, A. Di Carlo and P. Lugli, "Monte Carlo simulation of electrons dynamics in superlattice quantum cascade laser," *Appl. Phys. Lett.*, vol. 80, pp. 920-922, 2002.
- [14] A. Demic, A. Grier, Z. Ikonic, A. Valavanis, C.A. Evans, R. Mohandas, L. H. Li, E. H. Linfield, A. G. Davies and D. Indjin, "Infinite-period density-matrix model for terahertz-frequency quantum cascade lasers," *IEEE Trans. THz Sci. Technol.*, vol. 7, pp. 368-377, 2017.
- [15] R. Terazzi and J. Faist, "A density matrix model of transport and radiation in quantum cascade lasers," *New Journal of Physics*, vol. 12, pp. 033045, 2010.
- [16] H. Yasuda, T. Kubis, P. Vogl, N. Sekine, I. Hosako and K. Hirakawa, "Nonequilibrium Green's function calculation for four-level scheme terahertz quantum cascade lasers," *Appl. Phys. Lett.*, vol. 94, pp. 151109, 2009.
- [17] A. Wacker, "Gain in quantum cascade lasers and superlattices: a quantum transport theory," *Phys. Rev. B*, vol. 66, pp. 085326, 2002.
- [18] G. Agnew, A. Grier, T. Taimre, Y.L.Lim, M. Nikolic, A. Valavanis, J. Cooper, P. Dean, S. P. Khanna, M. Lachab, E. H. Linfield, A. G. Davies, P. Harrison, Z. Ikonic, D. Indjin and A. D. Rakić, "Efficient prediction of terahertz quantum cascade laser dynamics from steady-state simulations," *Appl. Phys. Lett.*, vol. 106, pp. 161105, 2015.
- [19] G. Agnew, A. Grier, T. Taimre, K. Bertling, Y.L.Lim, Z. Ikonic, P. Dean, A. Valavanis, P. Harrison, D. Indjin and A. D. Rakić, "Temperature-dependent high-speed dynamics of terahertz quantum cascade lasers", *IEEE J. Sel. Top. Quantum Electron.* vol. 23, pp. 1200209, 2017.
- [20] B. S. Williams, S. Kumar, Q. Hu and J. L. Reno, "Operation of terahertz quantum-cascade lasers at 164 K in pulsed mode and at 117 K in continuous-wave mode," *Opt. Express*, vol. 13, pp. 3331-3339, 2005.
- [21] S. Kohen, B. S. Williams and Q. Hu, "Electromagnetic modeling of terahertz quantum cascade laser waveguides and resonator," *J. Appl. Phys.*, vol. 97, pp. 053106, 2005.
- [22] E. Dupont, S. Fatholouloumi and H. C. Liu, "Simplified density-matrix model applied to three-well terahertz quantum cascade lasers," *Phys. Rev. B*, vol. 81, pp. 205311, 2010.
- [23] R. Terazzi and J. Faist, "A density matrix model of transport and radiation in quantum cascade lasers", *New Journal of Physics*, vol. 12, pp. 033045, 2010.
- [24] P. Tzenov, D. Burghoff, Q. Hu and C. Jirauschek, "Time domain modeling of terahertz quantum cascade lasers for frequency comb generation," *Opt. Express*, vol. 24, 23235, 2016.
- [25] X. Qi, I. Kundu, P. Dean, G. Agnew, T. Taimre, A. Valavanis, A. T. Grier, E. H. Linfield, A. G. Davies, D. Indjin and A. D. Rakić, "Mode-selection and tuning mechanisms in coupled-cavity terahertz quantum cascade lasers," *IEEE J. Sel. Top. Quantum Electron.* vol. 23, pp. 1200312, 2017.
- [26] C. Jirauschek and T. Kubis, "Modeling techniques for quantum cascade lasers," *Applied Physics Review*, vol. 1, 011307, 2017.
- [27] M. Xia and H. Ghafouri-Shiraz, "Quantum transmission line modelling method and its application in quantum dot amplifiers", *IEEE J. Quantum Electron.*, vol. 52, pp. 5100107, 2016.
- [28] M. Xia, H. Ghafouri-Shiraz, "Wavelength-dependent femtosecond pulse amplification in wideband tapered-waveguide quantum well semiconductor optical amplifiers," *Applied Optics*, vol. 54, pp. 10524-10531, 2015.
- [29] W. J. R. Hofer, "The transmission-line matrix method-theory and application," *IEEE Trans. Microw. Theory Tech.* vol. MTT-33, pp. 882-893, 1985.
- [30] P. B. Johns and R. L. Beurle, "Numerical solution of 2-dimensional scattering problems using a transmission-line matrix," *Proc. Inst. Elect. Eng.*, vol. 118, pp. 1203-1208, 1971.
- [31] I. Kundu, P. Dean, A. Valavanis, H. L. Li, Y. J. Han, E. H. Edmund and A. G. Davies, "Frequency tunability and spectral control in terahertz quantum cascade lasers with phase-adjusted finite-defect-site photonic lattices," *IEEE Trans. THz Sci. Technol.*, vol. 7, pp. 360-367, 2017.
- [32] F. Friederich, G. Schuricht, A. Deninger, F. Lison, G. Spickermann, P. H. Bolívar and H. G. Roskos, "Phase-locking of the beat signal of two distributed-feedback diode lasers to oscillators working in the MHz to THz range," *Opt. Express*, vol. 18, pp. 8621-8629, 2010.
- [33] Y. L. Lim, P. Dean, M. Nikolić, R. Kliese, S. P. Khanna, M. Lachab, A. Valavanis, D. Indjin, Z. Ikonic, P. Harrison, E. H. Linfield, A. G. Davies, S. J. Wilson, and A. D. Rakić, "Demonstration of a self-mixing displacement sensor based on terahertz quantum cascade lasers," *Appl. Phys. Lett.*, vol. 99, pp. 081108, 2011.
- [34] M. Wienold, L. Schrottke, M. Giehler, R. Hey, W. Anders and H.T. Grahn, "Low-voltage terahertz quantum-cascade lasers based on LO-phonon-assisted interminiband transitions," *Electron. Lett.*, vol. 45, pp. 1030-1031, 2009.
- [35] S. L. Chuang, "Physics of optoelectronic devices," Wiley, New York, 2009.
- [36] P. Harrison and A. Valavanis, "Quantum wells, Wires and Dots (4<sup>th</sup> Edition)," Wiley, New York, 2016.
- [37] H. Ghafouri-Shiraz, *The Principles of Semiconductor Laser Diodes and Amplifiers: Analysis and Transmission Line Laser Modeling*. London, U.K.: Imperial College Press, 2004.
- [38] A. Yariv, *Quantum Electronics*, 3rd ed. (Wiley, 1989).
- [39] A. J. Lowery, "New inline wideband dynamic semiconductor laser amplifier model," *IEE Proc. Pt. J. Optoelectron.* vol. 135, pp. 242-250, 1988.
- [40] H. Li, J. C. Cao and H. C. Liu, "Effects of design parameters on the performance of terahertz quantum-cascade lasers," *Semicond. Sci. Technol.* vol. 23, 125040, 2008.
- [41] D. Oustinov, N. Jukam, R. Rungsawang, J. Madeo, S. Barbieri, P. Filloux, C. Sirtori, X. Marcadet, J. Tignon and S. Dhillon, "Phase seeding of a terahertz quantum cascade laser", *Nat. Commun.* vol. 69, pp. 1-6, 2010.
- [42] I. Kundu, F. Wang, X. Qi, H. Nong et al. "Ultrafast switch-on dynamics of frequency tuneable semiconductor lasers," *Nat. Commun.* vol. 9, pp. 1-8, 2018.
- [43] I. Kundu, P. Dean, A. Valavanis, J. R. Freeman, M. C. Rosamond, L. H. Li, Y. J. Han, E. H. Linfield and A. G. Davies, "Continuous frequency tuning with near constant output power in coupled Y-branched terahertz quantum cascade lasers with photonic lattice", *ACS Photonics*, vol. 5, pp. 2912-2920, 2018.